Electrical & Computer Engineering Faculty Publications

Department of Electrical and Computer Engineering

1-1-2008

Cooperative Localization Bounds for Indoor Ultra-Wideband Wireless Sensor Networks

Nayef Alsindi

Kaveh Pahlavan
Worcester Polytechnic Institute, kaveh@wpi.edu

Follow this and additional works at: http://digitalcommons.wpi.edu/electricalcomputerengineering-pubs

Part of the Electrical and Computer Engineering Commons

Research Article

Cooperative Localization Bounds for Indoor Ultra-Wideband Wireless Sensor Networks

Nayef Alsindi and Kaveh Pahlavan

Center for Wireless Information Network Studies, Electrical and Computer Engineering Department,
Worcester Polytechnic Institute, Worcester, MA 01609, USA

Correspondence should be addressed to Nayef Alsindi, nalsindi@wpi.edu

In recent years there has been growing interest in ad-hoc and wireless sensor networks (WSNs) for a variety of indoor applications. Localization information in these networks is an enabling technology and in some applications it is the main sought after parameter. The cooperative localization performance of WSNs is constrained by the behavior of the utilized ranging technology in dense cluttered indoor environments. Recently, ultra-wideband (UWB) Time-of-Arrival (TOA) based ranging has exhibited potential due to its large bandwidth and high time resolution. The performance of its ranging and cooperative localization capabilities in dense indoor multipath environments, however, needs to be further investigated. Of main concern is the high probability of non-line of sight (NLOS) and Direct Path (DP) blockage between sensor nodes which biases the TOA estimation and degrades the localization performance. In this paper, based on empirical models of UWB TOA-based Outdoor-to-Indoor (OTI) and Indoor-to-Indoor (ITI) ranging, we derive and analyze cooperative localization bounds for WSNs in different indoor multipath environments: residential, manufacturing floor, old office and modern office buildings. First, we highlight the need for cooperative localization in indoor applications. Then we provide comprehensive analysis of the factors affecting localization accuracy such as network and ranging model parameters.

1. INTRODUCTION

In recent years, there has been a growing interest in ad hoc and wireless sensor networks (WSNs) for a variety of applications. The development of MEMS technology and the advancement in digital electronics and wireless communications have made it possible to design small-size, low-cost, energy-efficient sensor nodes that could be deployed in different environments and serve various applications [1]. Localization information in WSNs is an enabling technology since sensor nodes deployed in an area, in general, require position information for routing, energy management, and application-specific tasks such as temperature, pressure monitoring, and so on [2]. In certain applications, WSNs are deployed to aid and improve localization accuracy in environments where the channel condition poses a challenge to range estimation [3]. In these environments, cooperative localization provides potential for numerous applications in the commercial, public safety, and military sectors [3, 4]. In commercial applications, there is a need to localize and track inventory items in warehouses, materials, and equipment in manufacturing floors, elderly in nursing homes, medical equipment in hospitals, and objects in residential homes. In public safety and military applications, indoor localization systems are needed to track inmates in prisons and navigate policemen, fire fighters, and soldiers to complete their missions inside buildings [4].

In these indoor cooperative localization applications, a small number (M) of sensors called anchors are deployed outside surrounding a building where they obtain their location information via GPS or are preprogramed during setup. The N unlocalized sensor nodes are then deployed inside the building, for example, fire fighters or soldiers entering a hostile building, who with the help of the M anchors attempt to obtain their own location information. In traditional approaches, such as trilateration (triangulation)
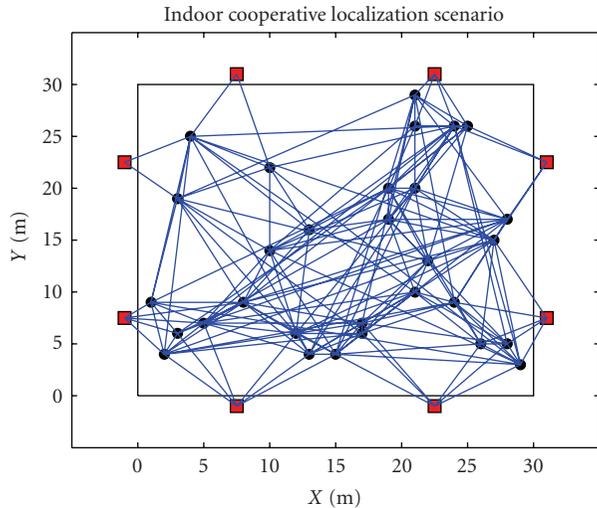
FIGURE 1: Indoor cooperative localization application. Squares are anchor nodes and circles are sensor nodes. Connectivity based on Fuller models at 500 MHz.

techniques, the exterior anchor nodes usually fail to cover a large building which makes localization ineffective. In addition, the problems of indoor multipath and non-line-of-sight (NLOS) channel conditions further degrade the range estimates yielding unreliable localization performance [4]. Implementation of the cooperative localization approach, see Figure 1, extends the coverage of the outside anchors to the inside nodes and has the ability to enhance localization accuracy through the availability of more range measurements between the sensor nodes.

Effective cooperative localization in indoor WSNs does, however, hinge on the ranging technology. Among the emerging techniques, ultra-wideband (UWB) time-of-arrival-(TOA) based ranging has recently received considerable attention [5–7]. In addition to its high data rate communications, it has been selected as a viable candidate for precise ranging and localization. This is mainly due to its large system bandwidth which offers high resolution and signaling that allows for centimeter accuracies, low-power and low-cost implementation [5–8]. The performance of this technique depends on the availability of the direct-path (DP) signal between a pair of sensor nodes [9, 10]. In the presence of the DP, that is, short-distance line-of-sight (LOS) conditions, accurate UWB TOA estimates in the range of centimeters are feasible due to the high time-domain resolution [11–14]. The challenge, however, is UWB ranging in indoor NLOS conditions which can be characterized as dense multipath environments [9, 10]. In these conditions, the DP between a pair of nodes can be blocked with high probability, substantially degrading the range and localization accuracy. Therefore, there is a need to analyze the impact of these channel limitations on the performance of cooperative localization in indoor WSNs.

Evaluation of localization bounds in multihop WSNs has been examined extensively [15–17], where the focus has been on analyzing the impact of network parameters such

as the number of anchors, node density, and deployment topology affecting localization accuracy. These localization bounds, however, have been analyzed with unbiased ranging assumptions between sensor nodes. In [18, 19], the impact of biased TOA range measurements on the accuracy of location estimates is investigated for cellular network applications. Their approach assumes NLOS induced errors as small perturbations, which clearly is not the case in indoor environments. A comprehensive treatment of the impact of biases on the wireless geolocation accuracy in NLOS environments is reported in [20]. Recently, position error bounds for dense cluttered indoor environments have been reported in [21, 22] where the impact of the channel condition on the localization error is further verified in traditional localization.

In this paper, based on empirical UWB TOA-based outdoor-to-indoor (OTI) and indoor-to-indoor (ITI) ranging models in different indoor building environments reported in [23–25], we extend the analysis of localization bounds in NLOS environments [20] to cooperative localization in indoor multihop WSNs. We focus on fire-fighter or military operation application where we analyze the fundamental limitations imposed by the indoor dense cluttered environment. Specifically, we analyze the impact of the channel-modeling parameters such as ranging coverage, statistics of the ranging error, probability of NLOS, and probability of DP blockage on localization accuracy. This modeling framework is necessary since OTI channel behavior affects anchor-node range estimation while ITI affects the node-node ranges. We first show that for the aforementioned indoor localization application, where traditional multilateration fails, cooperative localization, besides providing localization for the entire network, has the potential to further enhance the accuracy. We then evaluate the factors affecting localization accuracy, namely, network and channel-modeling parameters in different indoor environments: residential, manufacturing floor, old, and modern office buildings. To the authors knowledge, indoor channel-ranging model-specific cooperative localization bounds in WSNs are novel and provide comprehensive insight into the fundamental limitations facing indoor UWB TOA-based localization in both traditional and sensor networks.

The organization of the paper is as follows. In Section 2, we introduce the UWB TOA-based ranging models for indoor environments. In Section 3, using these models, we derive the generalized Cramer-Rao lower bound (G-CRLB) for cooperative localization in indoor multihop WSNs. In Section 4, we provide results of simulation which highlight the network and ranging channel-modeling parameters that affect the localization accuracy. Finally, we conclude the paper in Section 5.

2. TOA-BASED RANGING IN INDOOR MULTIPATH ENVIRONMENTS

2.1. Ranging coverage

One of the major factors determining the quality of TOA-based ranging and localization in indoor environments is

TABLE 1: UWB pathloss modeling parameters.

| Scenario | Environment | PL_p(dB) | Direct path | | | | Total signal | |
| | | | 500 MHz | | 3 GHz | | | |
			γ	χ (dB)	γ	χ (dB)	γ	χ (dB)
ITI	Fuller (LOS)	0	3.2	8.9	3.3	7.1	2.4	5.5
	Norton (LOS/NLOS)	0	3.5	8.5	4.5	9.1	2.6	3.4
	Fuller (NLOS)	10	4.1	8.3	4.5	8.7	3.3	5.8
	Schussler (NLOS)	6	3.4	7.9	4.0	8.4	3.0	4.6
	AK (NLOS)	7.5	5.4	6.2	5.6	8.5	3.6	6.2
OTI	Fuller	14.3	3.4	13.7	3.7	14.1	2.2	7.7
	Norton	8.7	3.9	7.8	5.0	10.1	3.3	4.4
	Schussler	7.6	4.1	10.5	4.2	11.1	3.2	6.1
	AK	10	4.6	8.7	5.1	8.9	3.1	3.2

the ability to detect the DP between a pair of sensor nodes in dense cluttered multipath conditions. For the indoor multipath channel, the impulse response is usually modeled as

$$h(\tau) = \sum_{k=1}^{L_p} \alpha_k e^{j\phi_k} \delta(\tau - \tau_k), \qquad (1)$$

where L_p is the number of multipath components (MPCs), and α_k, ϕ_k, and τ_k are amplitude, phase, and propagation delay of the kth path, respectively [26]. When the DP is detected, $\alpha_1 = \alpha_{DP}$ and $\tau_1 = \tau_{DP}$, where α_{DP} and τ_{DP} denote the DP amplitude and propagation delay, respectively. The distance between a pair of nodes is then $d_{DP} = v \times \tau_{DP}$, where v is the speed of signal propagation. In the absence of the DP, TOA-based ranging can be achieved using the amplitude and propagation delay of the first nondirect path (NDP) component given by α_{NDP} and τ_{NDP}, respectively. This results in a longer distance estimate given by $d_{NDP} = v \times \tau_{NDP}$, where $d_{NDP} > d_{DP}$. For a node's receiver to identify the DP, the ratio of the strongest MPC to the DP given by [27]

$$\rho_1 = \left(\frac{\max\left(|\alpha_k|\big|_{k=1}^{L_p}\right)}{|\alpha_{DP}|} \right) \qquad (2)$$

must be less than the receiver dynamic range ρ and the power of the DP must be greater than the receiver sensitivity κ. These constraints are given by

$$\rho_1 \leq \rho, \qquad (3a)$$

$$P_{DP} > \kappa, \qquad (3b)$$

where $P_{DP} = 20 \log_{10}(|\alpha_{DP}|)$. The performance of UWB TOA-based ranging is then constrained by the maximum feasible distance, where P_{DP} can satisfy (3a) and (3b). This is analogous to the dependence of a communication system's performance on the distance relationship of the total signal energy of all the detectable MPCs, or $P_T = 20 \log_{10}(\sum_{k=1}^{L_p} |\alpha_k|)$. In indoor environments, the distance-dependence of P_T, which determines the limitations of

communication coverage, is usually predicted from experimental pathloss models of the total signal energy in different environments and scenarios [28–30]. Similarly, the distance-dependence behavior of P_{DP} is important in analyzing the physical limitations facing UWB TOA-based ranging. The first comprehensive analysis of the UWB pathloss behavior of the DP between a pair of nodes has been experimentally reported in [23]. Following the analysis in [23], for a given system dynamic range, ρ, ranging coverage, R_c, is then defined as the distance in which the maximum tolerable average pathloss of the DP is within ρ. This is represented by

$$\max\{\overline{PL_{DP}}\} = 10\gamma \log_{10}(R_c) \leq \rho, \qquad (4)$$

where $\overline{PL_{DP}}$ is the average pathloss of the DP. The pathloss of the DP at some distance d, in decibels, is

$$PL_{DP}(d) = PL_0 + PL_p + 10\gamma \log_{10}\left(\frac{d}{d_0}\right) + \chi, \quad d \geq d_0, \qquad (5)$$

where PL_0 is the pathloss at $d_0 = 1$ m, $10\gamma \log_{10}(d/d_0)$ is the average pathloss with reference to d_0, PL_p is the penetration loss, γ is the pathloss exponent, and χ is the lognormal shadow fading. These parameters vary significantly for ITI and OTI rangings. The pathloss behavior of the DP is distance-dependant but because of attenuation and energy removed by scattering, its intensity decreases more rapidly with distance compared to the total signal energy [31]. This means that for a typical indoor multipath scattering environment, ranging coverage is less than communication coverage or $R_c < C_c$. This implies that although it is still feasible to communicate after R_c, the performance of TOA-based ranging is substantially degraded due to large TOA estimation errors that occur with high probability. Empirical UWB pathloss models of the DP in different ranging environments and scenarios are reported in [23] and provided in Table 1.

In general, ranging coverage in indoor multipath environments depends on the channel condition between a pair of nodes. The channel condition is physically constrained by

the environment and the scenario. The environment refers to the type of building such as residential, manufacturing, or office. The scenario refers to the relative location of the node-node or anchor-node pair which can be grouped into the following: ITI, OTI, and roof-to-indoor (RTI). In ITI ranging, the pathloss behavior varies significantly between LOS and NLOS channel conditions. In the latter, ranging coverage is reduced due to penetration loss caused by the interior wall structures, which results in a higher DP pathloss exponent. Similarly, OTI and RTI ranging imposes harsher constraints on the pathloss, due to the DP having to penetrate the outside walls and roof, respectively, which means that $R_c^{ITI} > R_c^{OTI} > R_c^{RTI}$ [23]. This poses a challenge specifically for indoor localization in ad hoc and WSN applications.

2.2. Ranging error

2.2.1. Overview

Before proceeding with derivation of the theoretic limits of cooperative localization in indoor environments, it is necessary to address the behavior of UWB TOA-based ranging errors. In addition to ranging coverage, localization bounds in indoor multipath channels are further constrained by the statistics of ranging error. The behavior of ranging error between a pair of nodes depends on the availability of the DP and, in the case of its absence, on the statistics of the blockage. In this paper, we categorize the error based on the following ranging states. In the presence of the DP, nodes must be within R_c which means that both (3a) and (3b) are met and the distance estimate is very accurate yielding

$$\hat{d}_{DP} = d_{DP} + \varepsilon_{DP} + z, \quad d \le R_c, \tag{6a}$$

$$\varepsilon_{DP} = \begin{cases} b_m(\omega) & \text{LOS}, \\ b_m(\omega) + b_{pd} & \text{NLOS}, \end{cases} \tag{6b}$$

where $b_m(\omega)$ is the bias induced by the multipath that dominates when the DP is present and it is a function of the system bandwidth ω [13, 14]. b_{pd} is the propagation delay imposed by the NLOS condition and z is zero mean measurement noise. Similar to wireless communications terminology, we will use the NLOS term to denote the absence of a *physical* LOS between the transmitter and the receiver and *not* the absence of the DP. This means that in NLOS the DP can be detected, albeit attenuated. When a sensor node is within R_c but experiences sudden blockage of the DP, also known as undetected direct path (UDP) [10], (3a) is not met and the DP is shadowed by some obstacle burying its power under the dynamic range of the receiver. This concept is very similar to deep fading that occurs in communications where the performance in a certain location within communication coverage is degraded. This type of fading in ranging applications occurs when sensor nodes are separated by obstacles such as metallic doors, multiple walls, cabinets or even elevators, and metallic studs. In this situation, the ranging estimate experiences a larger bias error compared to (6). Emphasizing that ranging is achieved
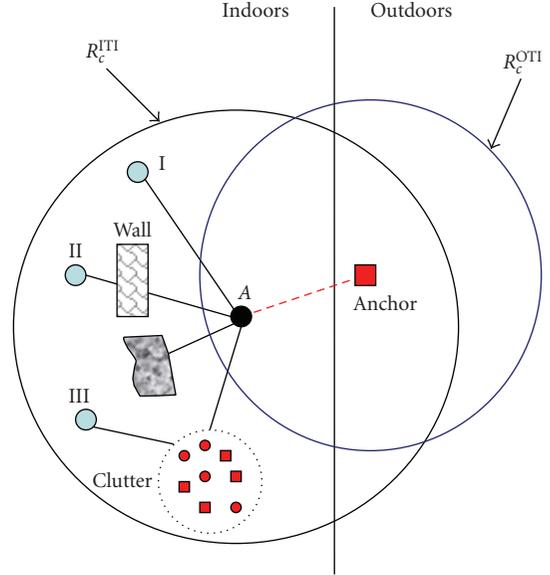

FIGURE 2: OTI/ITI ranging coverage and the associated ranging error conditions, I: λ (LOS), II: η (NLOS-DP), III: β (NLOS-NDP).

through the first NDP component, the estimate is then given by

$$\hat{d}_{NDP} = d_{DP} + \varepsilon_{NDP} + z, \quad d \le R_c, \tag{7a}$$

$$\varepsilon_{NDP} = b_m(\omega) + b_{pd} + b_B(\omega), \tag{7b}$$

where $b_B(\omega)$ is positive additive bias representing the nature of the blockage, which dominates the error compared to measurement noise and multipath bias. The dependency of $b_B(\omega)$ on the bandwidth is highlighted in the fact that higher bandwidth results in lower energy per MPC which increases the probability of DP blockage and reduces ranging coverage. Figure 2 further illustrates the different ranging states within ranging coverage. Finally, when the user operates outside of R_c neither (3a) nor (3b) is met and large TOA estimation errors occur with high probability. Formally, these ranging states can be defined as follows:

$$\zeta_1 = \{\hat{d} = \hat{d}_{DP} \mid d \le R_c\};$$
$$\zeta_2 = \{\hat{d} = \hat{d}_{NDP} \mid d \le R_c\};$$
$$\zeta_3 = \{\hat{d} = \hat{d}_{NDP} \mid d > R_c\};$$
$$\zeta_4 = \{\hat{d} = \hat{d}_{DP} \mid d > R_c\}. \tag{8}$$

In this paper, we will focus on deriving localization bounds for WSNs based on the error statistics within the ranging coverage, that is, ζ_1 and ζ_2, since the performance in ζ_3 is dominated by large measurement noise variations which means that the significance of (6b) and (7b) diminishes [21]. We further assume that $p(\zeta_4) \approx 0$ since, from our definition in (4), the DP cannot be detected after the ranging coverage.

2.2.2. Modeling the ranging error

For a range estimate between node pairs, the bias in (6) and (7) is unknown but deterministic since we assume the channel is quasistatic where the nodes and the obstacle are stationary. For a given building environment, the spatial behavior of the biases can be assumed random since the channel condition, that is, scattering and blocking obstacles, cannot be determined *a priori*. The biases in each of these channel conditions can then be treated as a random variable where their spatial distribution can provide statistical characterization of the severity of the indoor multipath channel.

The ranging error experienced in an indoor environment can then be modeled by combining the conditions in (6) and (7) through the following expression [24, 25]:

$$\varepsilon = b_m(\omega) + G \cdot (b_{pd} + X \cdot b_B(\omega)), \qquad (9)$$

where G is a Bernoulli random variable that distinguishes between the error in LOS and NLOS. That is,

$$G = \begin{cases} 0, & \text{LOS}, \\ 1, & \text{NLOS}, \end{cases} \qquad (10)$$

where $p(G = 0) = p(\text{LOS})$ and $p(G = 1) = p(\text{NLOS})$. Similarly, X is a Bernoulli random variable that models the occurrence of DP blockage given by

$$X = \begin{cases} 0, & \zeta_1, \\ 1, & \zeta_2, \end{cases} \qquad (11)$$

with $p(X = 1) = p(\zeta_2)$ denotes the probability of the occurrence of blockage, while $p(X = 0) = p(\zeta_1)$ denotes the probability of detecting a DP.

In order to facilitate the notations for the G-CRLB derivations, we assign specific variables for each of the channel conditions in (9), that is,

$$\varepsilon = \begin{cases} \lambda, & G = 0, X = 0, \\ \eta, & G = 1, X = 0, \\ \beta, & G = 1, X = 1. \end{cases} \qquad (12)$$

The probability density functions (PDFs) of these conditions, $f_\lambda(\lambda)$, $f_\eta(\eta)$, and $f_\beta(\beta)$, have been experimentally obtained through comprehensive UWB channel measurements for the different ranging environments and scenarios [24, 25]. For the LOS channel, the error was modeled as a normal distribution

$$f_\lambda(\lambda) = \frac{1}{\sqrt{2\pi\sigma_\lambda^2}} \exp\left[-\frac{(\lambda - \mu_\lambda)^2}{2\sigma_\lambda^2} \right] \qquad (13)$$

with mean μ_λ and standard deviation σ_λ specific to the LOS multipath induced errors. In NLOS scenarios, when the DP is present, the amount of propagation delay and multipath due to obstructing objects, such as wooden walls, causes the biases to be more positive. Accordingly, the ranging error

in this condition was modeled with a normal distribution similar to (13) but with higher mean and variance

$$f_\eta(\eta) = \frac{1}{\sqrt{2\pi\sigma_\eta^2}} \exp\left[-\frac{(\eta - \mu_\eta)^2}{2\sigma_\eta^2} \right]. \qquad (14)$$

Finally, in the absence of the DP, the error was best modeled by the lognormal distribution since only positive errors are possible in this condition [24, 25]. The PDF is given by

$$f_\beta(\beta) = \frac{1}{\beta\sqrt{2\pi\sigma_\beta^2}} \exp\left[-\frac{(\ln\beta - \mu_\beta)^2}{2\sigma_\beta^2} \right], \qquad (15)$$

where μ_β and σ_β are the mean and standard deviations of the ranging error logarithm.

The probability of DP blockage, $p(X = 1)$, and the parameters of the *normalized* ranging error PDFs were reported in [24, 25] and are reproduced in Tables 2–4. The UWB ranging coverage and error models will provide a realistic platform in which to analyze the G-CRLB and the localization accuracy in different indoor multipath environments.

3. INDOOR COOPERATIVE LOCALIZATION BOUNDS

3.1. Problem formulation

Based on the ranging models of Section 2, we derive the G-CRLB for cooperative localization in indoor WSNs. The scenario we consider is as follows. M anchor nodes are placed outside surrounding the building with coordinates given by $\boldsymbol{\theta}_A = (x_m, y_m)^T$, where $m \in [-M, 0]$ and T is the transpose operation. These anchors are GPS-equipped where they have knowledge of their position. We assume that they are synchronized and that their position errors are negligible (or even calibrated). The problem then is to localize N sensor nodes with unknown coordinates that are randomly scattered in the indoor environment, see Figure 1. The coordinates of the nodes to be estimated are given by $\boldsymbol{\theta} = (x_n, y_n)^T$, where $n \in [1, N]$. A 2-dimensional analysis will be provided, as extension to 3 dimensions is rather straightforward. Furthermore, connectivity between node-node and anchor-node is assumed if the range measurements are within ITI and OTI ranging coverages, R_c^{ITI} and R_c^{OTI}, respectively. Estimates beyond the ranging coverage will not be considered connected.

The range estimate between the ith and jth sensor nodes can then be given by

$$\hat{d}_{ij} = d'_{ij} + z_{ij}, \qquad (16)$$

where d'_{ij} is biased by one of the ranging conditions given in (12) or

$$d'_{ij} = d_{ij} + \begin{cases} \lambda_{ij}, & \text{LOS}, \\ \eta_{ij}, & \text{NLOS/DP}, \quad d_{ij} \le R_c \\ \beta_{ij}, & \text{NLOS/NDP}, \end{cases} \qquad (17)$$

TABLE 2: Probability of ζ_1 and ζ_2 in NLOS environments.

Scenario	Environment	500 MHz		3 GHz	
		% ζ_1	% ζ_2	% ζ_1	% ζ_2
ITI	Fuller	10	90	2	98
	Norton	96	4	83	17
	Schussler	89	11	87	13
	AK	39	61	32	68
OTI	Fuller	42	58	39	61
	Norton	57	43	24	76
	Schussler	77	23	60	40
	AK	40	60	22	78

TABLE 3: Gaussian distribution modeling parameters of the normalized ranging error. Subscripts denote the source of the ranging error.

Scenario	Environment	500 MHz		3 GHz	
		μ_m	σ_m	μ_m	σ_m
ITI	Fuller (LOS)	0	0.028	0	0.006
	Norton (LOS)	0	0.022	0	0.007
		$\mu_{m,pd}$	$\sigma_{m,pd}$	$\mu_{m,pd}$	$\sigma_{m,pd}$
	Fuller (NLOS)	0.058	0.028	0.003	0.01
	Schussler (NLOS)	0.029	0.047	0.014	0.016
	AK (NLOS)	0.023	0.020	0.009	0.004
OTI	Fuller	0.015	0.017	0.002	0.011
	Norton	0.019	0.029	0.002	0.015
	Schussler	0.041	0.045	0.011	0.013
	AK	0.034	0.023	0.012	0.004

and z_{ij} is the zero mean measurement noise between the sensors. d_{ij} is the actual distance between the sensor nodes and it is given by

$$d_{ij} = \sqrt{(x_i - x_j)^2 + (y_i - y_j)^2}, \qquad (18)$$

where x and y are the x- and y-coordinates, respectively. In the general case, an indoor WSN will be connected through R biased range measurements. Each $r \in [1, R]$ range measurement from node i to node j can be represented by $r \leftrightarrow (i, j)$. The range measurements are then stacked into a vector $\hat{\mathbf{d}} = (\hat{d}_1, \dots, \hat{d}_R)^T$, where $\hat{\mathbf{d}} = \mathbf{d} + \boldsymbol{\varepsilon} + \mathbf{z}$ and the corresponding bias vector is $\boldsymbol{\varepsilon} = (\varepsilon_1, \dots, \varepsilon_R)^T$. $\boldsymbol{\varepsilon}$ can be further decomposed into three subsets: L LOS, P NLOS/DP, and Q NLOS/NDP, or

$$\boldsymbol{\lambda} = (\lambda_1, \dots, \lambda_L)^T,$$
$$\boldsymbol{\eta} = (\eta_1, \dots, \eta_P)^T, \qquad (19)$$
$$\boldsymbol{\beta} = (\beta_1, \dots, \beta_Q)^T,$$

where $R = L + P + Q$. We further assume that it is possible to distinguish between these different ranging conditions through NLOS and DP blockage identification algorithms [32, 33]. Note that, even in LOS, our modeling assumption maintains the existence of bias due to multipath. This is usually neglected in LOS analysis, since single-path propagation is assumed [20]. The statistics of the multipath biases, obtained from measurements, are incorporated into the analysis to provide a realistic evaluation of the problem.

3.2. The generalized Cramer-Rao lower bound

The unknown vector of parameters to be estimated is obtained by combining the coordinates of the unknown nodes positions with the bias vector or by

$$\boldsymbol{\theta} = (x_1, y_1, \dots, x_N, y_N, \lambda_1, \dots, \lambda_L, \eta_1, \dots, \eta_P, \beta_1, \dots, \beta_Q)^T. \qquad (20)$$

The CRLB provides a lower bound on the variance of any unbiased estimate of the unknown parameters [34]. In the case the estimates are biased, it is possible to obtain the G-CRLB given that the statistics of the biases are available *a priori* [20, 34]. The empirical PDFs of $\boldsymbol{\lambda}$, $\boldsymbol{\eta}$, and $\boldsymbol{\beta}$, or $f_\lambda(\lambda)$, $f_\eta(\eta)$, and $f_\beta(\beta)$, respectively, were introduced in Section 2 and their distance-normalized parameters are presented in Tables 3-4.

The G-CRLB is then given by [34]

$$E\left[(\hat{\boldsymbol{\theta}} - \boldsymbol{\theta})(\hat{\boldsymbol{\theta}} - \boldsymbol{\theta})^T\right] \geq \mathbf{J}^{-1}, \qquad (21)$$

TABLE 4: Lognormal distribution modeling parameters of the normalized ranging error. Subscripts denote the source of the ranging error.

Scenario	Environment	500 MHz		3 GHz	
		$\mu_{m,\text{pd},B}$	$\sigma_{m,\text{pd},B}$	$\mu_{m,\text{pd},B}$	$\sigma_{m,\text{pd},B}$
ITI	Norton (NLOS)	−3.13	0.62	−4.29	0.45
	Fuller (NLOS)	−1.68	0.88	−1.90	1.13
	Schussler (NLOS)	−1.59	0.49	−2.72	0.53
	AK (NLOS)	−2.17	0.45	−2.89	0.81
OTI	Fuller	−2.33	0.75	−2.99	1.17
	Norton	−2.78	0.65	−3.82	0.52
	Schussler	−2.03	0.58	−3.16	0.45
	AK	−2.32	0.51	−3.11	0.77

where $E[\cdot]$ is the expectation operation and $\mathbf{J}$ is the information matrix that consists of two parts,

$$\mathbf{J} = \mathbf{J}_{\boldsymbol{\theta}} + \mathbf{J}_{\mathbf{P}}. \tag{22}$$

$\mathbf{J}_{\boldsymbol{\theta}}$ is the Fisher information matrix (FIM) which represents the *data* and $\mathbf{J}_{\mathbf{P}}$ represents the *a priori* information that reflects the statistics of the biases. Specifically, the *data* FIM can be obtained by evaluating

$$\mathbf{J}_{\boldsymbol{\theta}} = E_{\boldsymbol{\theta}}\left[\frac{\partial}{\partial \boldsymbol{\theta}} \ln f(\widehat{\mathbf{d}} \mid \boldsymbol{\theta}) \cdot \left(\frac{\partial}{\partial \boldsymbol{\theta}} \ln f(\widehat{\mathbf{d}} \mid \boldsymbol{\theta})\right)^T\right], \tag{23}$$

where $f(\widehat{\mathbf{d}} \mid \boldsymbol{\theta})$ is the joint PDF of the range measurement vector $\widehat{\mathbf{d}} = (\widehat{d}_1,\dots,\widehat{d}_R)^T$ conditioned on $\boldsymbol{\theta}$. Since the measurement noise is usually assumed zero mean Gaussian, the joint PDF can be given by

$$f(\widehat{\mathbf{d}} \mid \boldsymbol{\theta}) \propto \exp\left\{-\frac{1}{2}(\widehat{\mathbf{d}} - \mathbf{d}')\boldsymbol{\Lambda}(\widehat{\mathbf{d}} - \mathbf{d}')^T\right\}, \tag{24}$$

where $\boldsymbol{\Lambda}$ is the inverse of the measurements covariance matrix or $\boldsymbol{\Lambda}^{-1} = E[(\widehat{\mathbf{d}} - \mathbf{d}')(\widehat{\mathbf{d}} - \mathbf{d}')^T]$ and $\mathbf{d}'$ is the biased vector of the range measurements. Assuming that the measurements are uncorrelated, $\boldsymbol{\Lambda}$ is then diagonal with the elements given by $\boldsymbol{\Lambda} = \text{diag}(\sigma_{z_1}^{-2},\dots,\sigma_{z_R}^{-2})$. Since $f(\widehat{\mathbf{d}} \mid \boldsymbol{\theta})$ is a function of $\mathbf{d}'$ which is in turn a function of $\boldsymbol{\theta}$, $\mathbf{J}_{\boldsymbol{\theta}}$ can be obtained by the application of the chain rule or by

$$\mathbf{J}_{\boldsymbol{\theta}} = \left(\frac{\partial \mathbf{d}'}{\partial \boldsymbol{\theta}}\right) \cdot E_{\mathbf{d}'}\left[\left(\frac{\partial}{\partial \mathbf{d}'} \ln f(\widehat{\mathbf{d}} \mid \mathbf{d}')\right)\left(\frac{\partial}{\partial \mathbf{d}'} \ln f(\widehat{\mathbf{d}} \mid \mathbf{d}')\right)^T\right]$$
$$\cdot \left(\frac{\partial \mathbf{d}'}{\partial \boldsymbol{\theta}}\right)^T, \tag{25a}$$

$$\mathbf{J}_{\boldsymbol{\theta}} = \mathbf{H} \cdot \mathbf{J}_{\mathbf{d}'} \cdot \mathbf{H}^T, \tag{25b}$$

where $\mathbf{J}_{\mathbf{d}'}$ is the FIM but conditioned on $\mathbf{d}'$ and it is given by

$$\mathbf{J}_{\mathbf{d}'} = E_{\mathbf{d}'}\left[\frac{\partial}{\partial \mathbf{d}'} \ln f(\widehat{\mathbf{d}} \mid \mathbf{d}') \cdot \left(\frac{\partial}{\partial \mathbf{d}'} \ln f(\widehat{\mathbf{d}} \mid \mathbf{d}')\right)^T\right]. \tag{26}$$

The $\mathbf{H}$ matrix contains information regarding the geometry of the WSN connectivity and the condition of the biased range measurements. As a result, it can be decomposed into the three ranging conditions λ, η, and β given by

$$\mathbf{H} = \begin{pmatrix} \mathbf{H}_\lambda^1 & \mathbf{H}_\eta^1 & \mathbf{H}_\beta^1 \\ \vdots & \vdots & \vdots \\ \mathbf{H}_\lambda^N & \mathbf{H}_\eta^N & \mathbf{H}_\beta^N \\ \mathbf{I}_\lambda & 0 & 0 \\ 0 & \mathbf{I}_\eta & 0 \\ 0 & 0 & \mathbf{I}_\beta \end{pmatrix} \tag{27}$$

and it is a $(2 \times N + R) \times R$ matrix. The submatrix components are then given by

$$\mathbf{H}_\lambda^n = \begin{pmatrix} \dfrac{\partial d_{\lambda_1}'}{\partial x_n} & \cdots & \dfrac{\partial d_{\lambda_L}'}{\partial x_n} \\ \dfrac{\partial d_{\lambda_1}'}{\partial y_n} & \cdots & \dfrac{\partial d_{\lambda_L}'}{\partial y_n} \end{pmatrix}, \tag{28a}$$

$$\mathbf{H}_\eta^n = \begin{pmatrix} \dfrac{\partial d_{\eta_1}'}{\partial x_n} & \cdots & \dfrac{\partial d_{\eta_P}'}{\partial x_n} \\ \dfrac{\partial d_{\eta_1}'}{\partial y_n} & \cdots & \dfrac{\partial d_{\eta_P}'}{\partial y_n} \end{pmatrix}, \tag{28b}$$

$$\mathbf{H}_\beta^n = \begin{pmatrix} \dfrac{\partial d_{\beta_1}'}{\partial x_n} & \cdots & \dfrac{\partial d_{\beta_Q}'}{\partial x_n} \\ \dfrac{\partial d_{\beta_1}'}{\partial y_n} & \cdots & \dfrac{\partial d_{\beta_Q}'}{\partial y_n} \end{pmatrix}, \tag{28c}$$

for $n \in [1, N]$, and their respective dimensions are $(2 \times L)$, $(2 \times P)$, and $(2 \times Q)$. $\mathbf{I}_\lambda$, $\mathbf{I}_\eta$, and $\mathbf{I}_\beta$ are the identity matrices of order L, P, and Q, respectively. Elements of (28) will be nonzero when a range measurement is connected to node $(x_n, y_n)^T$ and zero otherwise. For example, if node 1 with coordinates $(x_1, y_1)^T$ is connected to node 2 with coordinates $(x_2, y_2)^T$ by the LOS range $d_{\lambda_1}' = \sqrt{(x_1 - x_2)^2 + (y_1 - y_2)^2} + \lambda_1$, then the respective element in (28a) is

$$\begin{pmatrix} \dfrac{\partial d_{\lambda_1}'}{\partial x_1} \\ \dfrac{\partial d_{\lambda_1}'}{\partial y_1} \end{pmatrix} = \begin{pmatrix} \dfrac{x_1 - x_2}{\sqrt{(x_1 - x_2)^2 + (y_1 - y_2)^2}} \\ \dfrac{y_1 - y_2}{\sqrt{(x_1 - x_2)^2 + (y_1 - y_2)^2}} \end{pmatrix}. \tag{29}$$

Similarly, $\mathbf{J}_{\mathbf{d}'}$ can be decomposed according to the ranging conditions, where

$$
\mathbf{J}_{\mathbf{d}'} = \begin{pmatrix} \boldsymbol{\Lambda}_\lambda & 0 & 0 \\ 0 & \boldsymbol{\Lambda}_\eta & 0 \\ 0 & 0 & \boldsymbol{\Lambda}_\beta \end{pmatrix} \tag{30}
$$

is an $R \times R$ matrix. Specifically, $\boldsymbol{\Lambda}_\lambda = \text{diag}(\sigma_{z_1}^{-2}, \ldots, \sigma_{z_L}^{-2})$, $\boldsymbol{\Lambda}_\eta = \text{diag}(\sigma_{z_1}^{-2}, \ldots, \sigma_{z_P}^{-2})$, and $\boldsymbol{\Lambda}_\beta = \text{diag}(\sigma_{z_1}^{-2}, \ldots, \sigma_{z_Q}^{-2})$. In this paper, our focus is on analyzing the impact of the biases due to multipath and DP blockage and, in reality, the measurement noise time variations in these different ranging conditions might not differ significantly for a high system dynamic range [35]. As a result, we will assume equal noise variance, that is, $\boldsymbol{\Lambda}_\lambda = \boldsymbol{\Lambda}_\eta = \boldsymbol{\Lambda}_\beta$. $\mathbf{J}_{\boldsymbol{\theta}}$ can then be obtained by substituting (27) and (30) into (25b) or

$$
\mathbf{J}_{\boldsymbol{\theta}} = \begin{pmatrix} \mathbf{H}_\lambda^1 & \mathbf{H}_\eta^1 & \mathbf{H}_\beta^1 \\ \vdots & \vdots & \vdots \\ \mathbf{H}_\lambda^N & \mathbf{H}_\eta^N & \mathbf{H}_\beta^N \\ \mathbf{I}_\lambda & 0 & 0 \\ 0 & \mathbf{I}_\eta & 0 \\ 0 & 0 & \mathbf{I}_\beta \end{pmatrix} \cdot \begin{pmatrix} \boldsymbol{\Lambda}_\lambda & 0 & 0 \\ 0 & \boldsymbol{\Lambda}_\eta & 0 \\ 0 & 0 & \boldsymbol{\Lambda}_\beta \end{pmatrix} \cdot \begin{pmatrix} \mathbf{H}_\lambda^1 & \mathbf{H}_\eta^1 & \mathbf{H}_\beta^1 \\ \vdots & \vdots & \vdots \\ \mathbf{H}_\lambda^N & \mathbf{H}_\eta^N & \mathbf{H}_\beta^N \\ \mathbf{I}_\lambda & 0 & 0 \\ 0 & \mathbf{I}_\eta & 0 \\ 0 & 0 & \mathbf{I}_\beta \end{pmatrix}^T
$$

$$
= \begin{pmatrix} \boldsymbol{\Gamma} & \cdots & \boldsymbol{\Gamma}' & \mathbf{H}_\lambda^1 \boldsymbol{\Lambda}_\lambda & \mathbf{H}_\eta^1 \boldsymbol{\Lambda}_\eta & \mathbf{H}_\beta^1 \boldsymbol{\Lambda}_\beta \\ \vdots & \ddots & \vdots & \vdots & \vdots & \vdots \\ \boldsymbol{\Gamma}'' & \cdots & \boldsymbol{\Gamma}''' & \mathbf{H}_\lambda^1 \boldsymbol{\Lambda}_\lambda & \mathbf{H}_\eta^1 \boldsymbol{\Lambda}_\eta & \mathbf{H}_\beta^1 \boldsymbol{\Lambda}_\beta \\ \boldsymbol{\Lambda}_\lambda (\mathbf{H}_\lambda^1)^T & \cdots & \boldsymbol{\Lambda}_\lambda (\mathbf{H}_\lambda^N)^T & \boldsymbol{\Lambda}_\lambda & 0 & 0 \\ \boldsymbol{\Lambda}_\eta (\mathbf{H}_\eta^1)^T & \cdots & \boldsymbol{\Lambda}_\eta (\mathbf{H}_\eta^N)^T & 0 & \boldsymbol{\Lambda}_\eta & 0 \\ \boldsymbol{\Lambda}_\beta (\mathbf{H}_\beta^1)^T & \cdots & \boldsymbol{\Lambda}_\beta (\mathbf{H}_\beta^N)^T & 0 & 0 & \boldsymbol{\Lambda}_\beta \end{pmatrix}, \tag{31}
$$

where $\boldsymbol{\Gamma}$ denotes $\mathbf{H}_\lambda^1 \boldsymbol{\Lambda}_\lambda (\mathbf{H}_\lambda^1)^T + \mathbf{H}_\eta^1 \boldsymbol{\Lambda}_\eta (\mathbf{H}_\eta^1)^T + \mathbf{H}_\beta^1 \boldsymbol{\Lambda}_\beta (\mathbf{H}_\beta^1)^T$, $\boldsymbol{\Gamma}'$ denotes $\mathbf{H}_\lambda^1 \boldsymbol{\Lambda}_\lambda (\mathbf{H}_\lambda^N)^T + \mathbf{H}_\eta^1 \boldsymbol{\Lambda}_\eta (\mathbf{H}_\eta^N)^T + \mathbf{H}_\beta^1 \boldsymbol{\Lambda}_\beta (\mathbf{H}_\beta^N)^T$, $\boldsymbol{\Gamma}''$ denotes $\mathbf{H}_\lambda^N \boldsymbol{\Lambda}_\lambda (\mathbf{H}_\lambda^1)^T + \mathbf{H}_\eta^N \boldsymbol{\Lambda}_\eta (\mathbf{H}_\eta^1)^T + \mathbf{H}_\beta^N \boldsymbol{\Lambda}_\beta (\mathbf{H}_\beta^1)^T$, and $\boldsymbol{\Gamma}'''$ denotes $\mathbf{H}_\lambda^N \boldsymbol{\Lambda}_\lambda (\mathbf{H}_\lambda^N)^T + \mathbf{H}_\eta^N \boldsymbol{\Lambda}_\eta (\mathbf{H}_\eta^N)^T + \mathbf{H}_\beta^N \boldsymbol{\Lambda}_\beta (\mathbf{H}_\beta^N)^T$. $\mathbf{J}_{\boldsymbol{\theta}}$ is a $(2 \times N + R) \times (2 \times N + R)$ matrix.

$\mathbf{J}_{\mathbf{P}}$, which contains the *a priori* statistics of the biases in (12), can be obtained by

$$
\mathbf{J}_{\mathbf{P}} = E\left[\frac{\partial}{\partial \boldsymbol{\theta}} \ln p_{\boldsymbol{\varepsilon}}(\boldsymbol{\varepsilon}) \cdot \left(\frac{\partial}{\partial \boldsymbol{\theta}} \ln p_{\boldsymbol{\varepsilon}}(\boldsymbol{\varepsilon}) \right)^T \right] \tag{32}
$$

and can be decomposed into the respective ranging conditions:

$$
\mathbf{J}_{\mathbf{P}} = \begin{pmatrix} 0 & 0 & 0 & 0 \\ 0 & \boldsymbol{\Omega}_\lambda & 0 & 0 \\ 0 & 0 & \boldsymbol{\Omega}_\eta & 0 \\ 0 & 0 & 0 & \boldsymbol{\Omega}_\beta \end{pmatrix}, \tag{33}
$$

where $\mathbf{J}_{\mathbf{P}}$ has the same order as $\mathbf{J}_{\boldsymbol{\theta}}$. Since the biases caused by scattering and DP blockage are dependant on the indoor architecture and the range estimates between different node pairs, the elements of (33) can be assumed independent.

With this assumption the elements of (33) are $\boldsymbol{\Omega}_\lambda = \text{diag}(\vartheta_1^{-2}, \ldots, \vartheta_L^{-2})$, $\boldsymbol{\Omega}_\eta = \text{diag}(\vartheta_1^{-2}, \ldots, \vartheta_P^{-2})$, and $\boldsymbol{\Omega}_\beta = \text{diag}(\vartheta_1^{-2}, \ldots, \vartheta_Q^{-2})$, where ϑ_r^{-2} is given by

$$
\vartheta_r^{-2} = -E\left[\frac{d^2}{d\varepsilon_r^2} \ln p_{\varepsilon_r}(\varepsilon_r) \right], \quad r \in [1, R]. \tag{34}
$$

From Section 2, λ and η were modeled with Gaussian distributions which means that ϑ_r^2 is the variance in the strict sense. β, however, is lognormally distributed, see (15), and evaluation of (34) is nontrivial but it can be shown to be

$$
\vartheta_q^{-2} = \exp\left[-2\mu_q + 2\sigma_q^2 \right] \times \left(1 + \frac{1}{\sigma_q^2} \right), \quad q \in [1, Q], \tag{35}
$$

where μ and σ are the mean and standard deviations of the ranging error logarithm. The G-CRLB for the N sensor nodes can then be obtained by computing $[\mathbf{J}^{-1}]_{(2 \times N) \times (2 \times N)}$ from (22) which is the first $(2 \times N) \times (2 \times N)$ diagonal submatrix of $[\mathbf{J}^{-1}]$.

4. SIMULATION RESULTS

4.1. Setup

The simulation setup is based on the application of fire fighters or soldiers requiring localization in indoor environments. M anchors are distributed evenly around the building where they are placed 1 m away from the exterior wall, see Figure 1. N sensor nodes are then uniformly distributed inside the building. Connectivity is assumed between node-node and anchor-node if the respective TOA range measurements are within ITI and OTI ranging coverage, R_c^{ITI} and R_c^{OTI}, respectively. The simulations were carried out for four different building environments: Fuller-modern office, Schussler-residential, Norton-manufacturing floor, and Atwater Kent (AK) old office. All these buildings are in Worcester, Mass. The UWB modeling parameters of these buildings were reported in [23–25] for two system bandwidths 500 MHz and 3 GHz and they are reproduced in Tables 1–4. The dynamic range of the system, ρ, is set to 90 dB and this parameter controls the ranging coverage and the number of internode range measurements in the WSN. For example, at 500 MHz bandwidth and 90 dB dynamic range, R_c^{ITI} will correspond roughly to 15–30 m depending on the LOS or NLOS condition and building environment. Similarly, R_c^{OTI} will be around 5–10 m depending on the building type. We set the measurement noise σ_z equal to 20 mm. For most simulations, unless otherwise stated, the probability of NLOS, $p(G = 1)$, was set to 0.5. The probability of blockage, $p(X = 1) = p(\zeta_2)$, however, was obtained from the measurement results in Table 2. The ranging conditions and the WSN internode connectivity are ultimately governed by the random variables G and X; see (9).

The models in Tables 3 and 4 are based on normalized ranging error $\psi = \varepsilon/d$. In order to compute $\mathbf{J}_{\mathbf{P}}$, the denormalized distributions, $f_\varepsilon(\varepsilon)$, must first be obtained, where $\varepsilon \in \{\lambda, \eta, \beta\}$. Thus for a given distance, d, the

denormalized distribution for one of the ranging conditions in (12) can be obtained by $f_\varepsilon(\varepsilon) = [f_\psi(\varepsilon/d)]/d$.

For the analysis of the simulations, we compute the average RMS of the location error of each WSN topology. The RMSE is computed by

$$\text{RMSE} = \frac{\sqrt{\text{tr}([\mathbf{J}^{-1}]_{(2\times N)\times(2\times N)})}}{N} = \frac{\sqrt{\sum_{i=1}^{N} \sigma_{x_i}^2 + \sigma_{y_i}^2}}{N}, \quad (36)$$

where $\text{tr}(\cdot)$ is the trace operation, $\sigma_{x_i}^2$ and $\sigma_{y_i}^2$ are the diagonal elements of the ith diagonal submatrix of $[\mathbf{J}^{-1}]_{(2\times N)\times(2\times N)}$. The average RMSE is obtained by averaging (36) over the total number of topologies and simulations.

4.2. Traditional versus cooperative localization

In traditional triangulation, only node-anchor range measurements are used and reliable 2-dimensional location information can only be obtained if a node is covered by at least 3 anchors. In the outdoor-indoor application, for a fixed R_c^{OTI}, the dimension of the building will dictate the fraction of nodes that can be localized. Calculation of G-CRLB in traditional localization uses the same formulation in Section 3 but only node-anchor range measurements are used. In order to verify the necessity and effectiveness of cooperative localization, we carried out 5000 Monte Carlo simulations with 100 different topologies and 50 simulations per topology for different D/R_c^{OTI} values. 500 MHz Fuller models were used with 4 anchors and 40 sensor nodes. We also assumed a square building that is $(D, D)^T$. Figure 3 provides the results of this simulation where the percentage of unlocalized nodes is plotted as a function of D/R_c^{OTI}. Figure 4 shows the average RMSE results. As expected, starting around $D/R_c^{\text{OTI}} = 1$, 10% of the nodes are unlocalized in traditional localization. As the size of the building increases, more nodes lose direct coverage to at least 3 of the outside anchors. By $D/R_c^{\text{OTI}} = 1.8$, triangulation is no longer possible. In comparison, cooperative localization is effective and provides position estimates for all the nodes. Moreover, Figure 4 shows that cooperative localization substantially outperforms the traditional counterpart. This means that for fire fighter/military applications, localization in indoor environments, especially in large buildings, cannot be achieved with triangulation alone. Cooperative localization will not only extend the coverage of the outside anchors to the inside nodes but it will enhance localization accuracy substantially as well. Further, for large building scenarios $D/R_c^{\text{OTI}} > 2$, more sensor nodes (i.e., greater node density) need to be deployed to maintain sufficient connectivity for effective cooperative localization.

4.3. Network parameters

In this subsection, we evaluate the impact of network parameters on localization accuracy. In the first experiment, we investigate the impact of node density. For the simulation, we fixed the number of anchors to 4 and the dimension of the building to $D = 25\,\text{m}$ and increased the number of nodes, that is, node density which is defined by $S =$

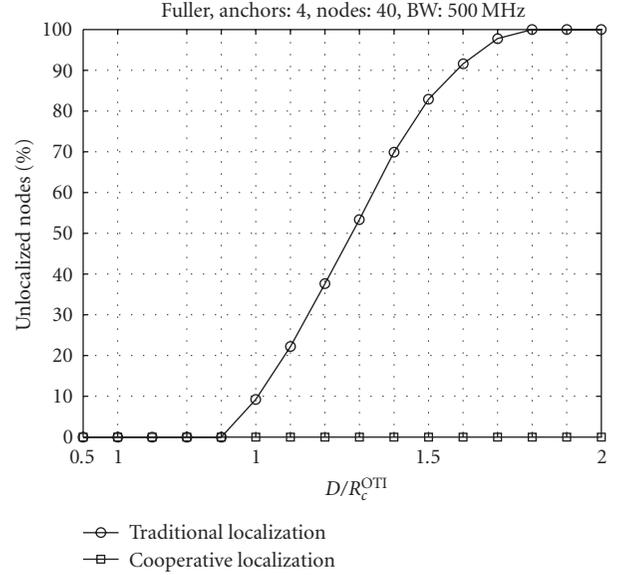FIGURE 3: Percentage of unlocalized sensor nodes as a function of D/R_c^{OTI}.

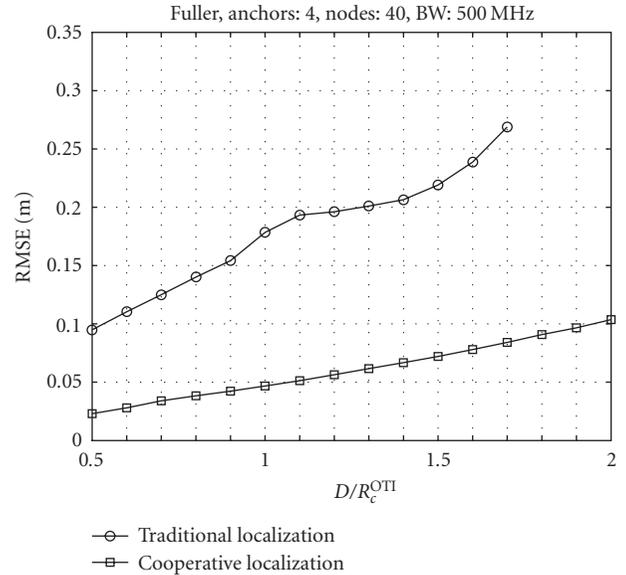
FIGURE 4: Traditional triangulation versus cooperative localization performance.

N/D^2. 5000 Monte Carlo simulations were carried out (50 different topologies and 100 simulations per topology). The latter is needed, since the ranging conditions and WSN connectivity are governed by Bernoulli random variables G and X. Figure 5 shows the simulated results for 500 MHz modeling parameters. Office buildings, AK and Fuller, exhibit the worst performance especially in sparse densities. Norton, a manufacturing floor, shows the best localization accuracy among the different buildings. This is expected since the manufacturing building interior is an open-space with cluttered machineries and metallic beams which is
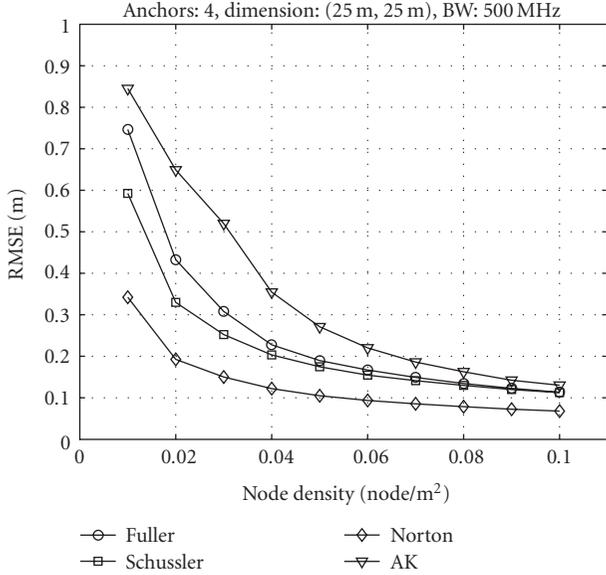
FIGURE 5: Localization performances as a function of node density in different indoor environments using 500 MHz models.

FIGURE 6: Localization performances as a function of number of anchors in different indoor environments using 500 MHz models.

reflected in the ranging coverage and error models. Further, the localizaiton bounds clearly indicate that the performance is dependant on ranging coverages, R_c^{ITI} and R_c^{OTI}, probability of DP blockage, $p(X = 1)$, and the respective error distributions $f_\varepsilon(\varepsilon)$; see Tables 1–4. Although AK has a lower ITI $p(X = 1)$ than Fuller, the performance in the former is worse due to shorter ITI ranging coverage. This can be seen by the difference in the pathloss exponents in Table 1. Shorter R_c^{ITI} means less internode range information and thus higher localization error.

Another important observation that can be concluded from this simulation is that the disadvantages of the indoor channel condition, ranging coverage, and error can be minimized by increasing node density. For instance, at 0.1 node/m², the difference in localization performance between the buildings diminishes significantly.

The impact of anchors on the localization accuracy is investigated in Figure 6. In this experiment, 5000 simulations were carried out with $D = 30$ m, $S = 0.03$ node/m², and the number of anchors was varied from 4 to 16 (anchors per side varies from 1 to 4). The results show that the effect of increasing the number of anchors is higher in the office buildings compared to the residential and manufacturing floor. This means that building environments with harsher indoor multipath channels (lower R_c^{ITI} and higher $p(G = 1)$ and $p(X = 1)$) require more anchors around the building for a fixed amount of sensor nodes to achieve similar localization performance as environments with "lighter" multipath channels. Finally, comparing both Figures 5 and 6, it is apparent that node density has a higher impact on the localization accuracy compared to the number of anchors. A similar observation was reported in [16] where localization error exhibited less sensitivity to the number of anchors.
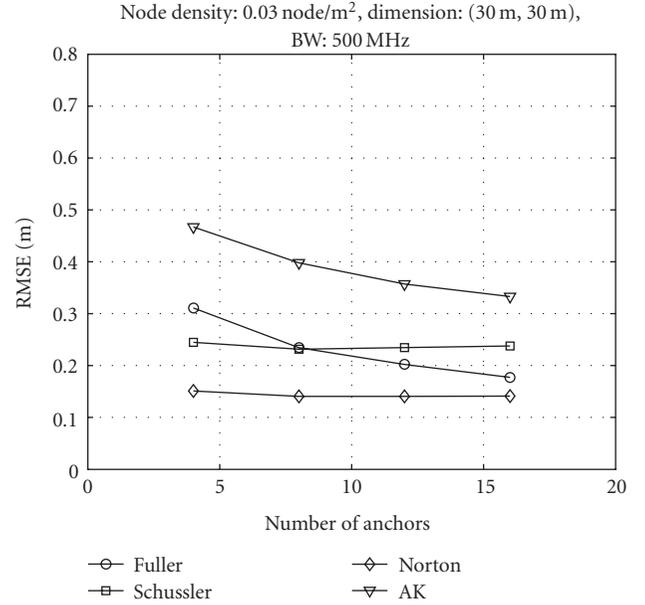
4.4. Ranging model parameters

In this subsection, we investigate the impact of the ranging model parameters: system dynamic range, ρ, $p(G = 1)$, and $p(X = 1)$ for 500 MHz and 3 GHz system bandwidths. First, we evaluate the localization bounds for different values of ρ which control both the R_c^{ITI} and R_c^{OTI}. In this experiment, the number of anchors is 4, $S = 0.04$ node/m² and the building dimension is $D = 30$ m. We ran 5000 Monte Carlo simulations (100 topologies and 50 simulations per topology). Figure 7 shows the simulated localization results as a function of dynamic range for different building environments and ranging models. The behavior of office buildings at 500 MHz is in general worse than residential and manufacturing buildings. However, at 3 GHz, the difference diminishes. Another interesting observation is that the impact of increasing the dynamic range eventually *saturates*. This means that after a certain dynamic range value all the nodes are connected to each other and no further gain can be achieved. The performance in buildings with higher ranging coverage tends to saturate earlier as seen when comparing AK with Norton or Schussler buildings.

The second experiment focuses on the impact of the probability of NLOS on the localization bounds where we varied $p(G = 1)$ experienced by the ITI ranges from 0 to 1. This does not affect OTI since it is always considered NLOS. $p(X = 1)$, however, was obtained from Table 2 and the respective ranging error distribution parameters from Tables 3 and 4. We ran 5000 Monte Carlo simulations (50 topologies and 100 simulations per topology). The number of anchors is 4, $S = 0.03$ node/m² and $D = 30$ m which means that N is around 34. The results are presented in Figure 8. The impact of multipath on localization error can be clearly seen
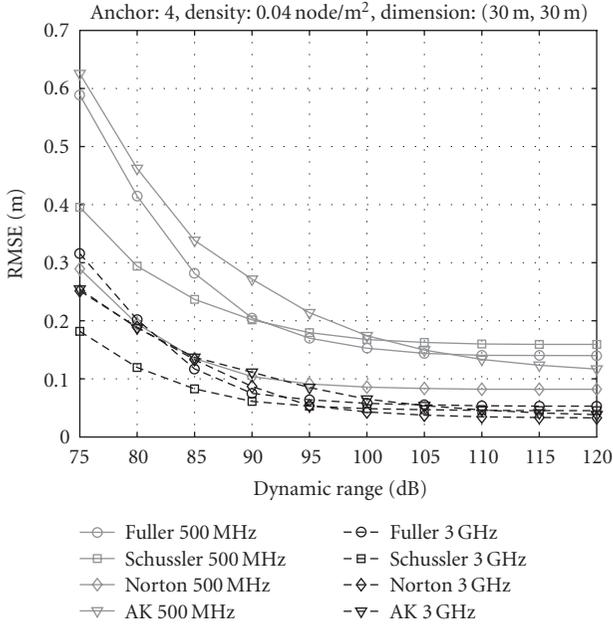
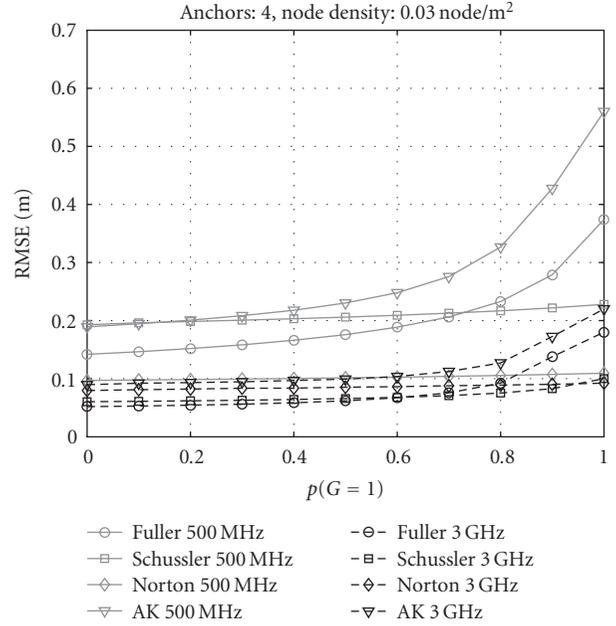Figure 7: Localization performances as a function of dynamic range, ρ, for 500 MHz and 3 GHz models.

Figure 8: Localization performances as a function of $p(G = 1)$ for 500 MHz and 3 GHz models.

for $p(G = 1) = 0$. Although the variance of the multipath bias models is dependant on the measurement campaign, it is important nonetheless to see that an average RMSE between 0.14–0.2 m can be caused by multipath alone for 500 MHz models. The effect of multipath, however, decreases substantially for the 3 GHz system bandwidth. As expected, increasing $p(G = 1)$ further degrades the localization performance in an indoor environment. The effect will be greater in buildings where $p(X = 1)$ is high. For example, both Fuller and AK NLOS channel models, see Table 2, exhibit rather high probabilities of DP blockage and this is reflected in the localization performance. Finally, Norton building is least impacted by NLOS because the blockage probability is low and the error statistics are significantly smaller than the other buildings.

Lastly, we investigate the impact of DP blockage probability. For the ranging error distributions given in Tables 3 and 4, we fix $p(G = 1) = 1$ and vary $p(X = 1)$ between 0 and 1. We ran 5000 Monte Carlo simulations (50 topologies and 100 simulations per topology). The number of anchors is 4, $S = 0.04$ node/m^2 and $D = 30$ m. The results are presented in Figure 9. For this specific experiment, results for AK were not available because $p(G = 1) = 1$, which means that the ITI ranges are always NLOS and thus shorter ranging coverage. In AK's case, the WSNs in all the simulations were ill connected. Nonetheless, the results in the other buildings show that increasing $p(X = 1)$ worsens the localization error. Norton is an exception, since the statistics of the ranging error in the presence and absence of the DP are close to each other (see Tables 3 and 4). The impact of blockage probability on office buildings is the highest, since the statistical distribution of the lognormal biases exhibits a higher "variance" compared to manufacturing or
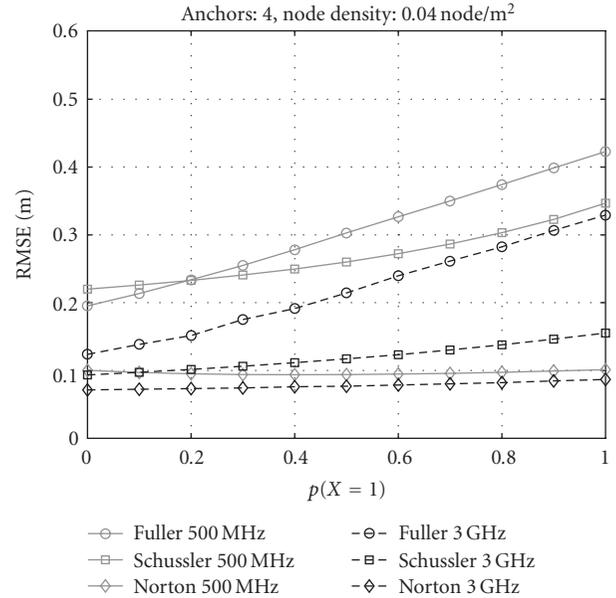

Figure 9: Localization performances as a function of DP blockage probability, $p(X = 1)$, for 500 MHz and 3 GHz models.

residential buildings. This can be seen in the Fuller model in Table 4 where such an environment exhibits a heavier tailed distribution of the spatial ranging errors [24, 25]. For these conditions, when the DP blockage occurs, a larger number of MPCs are lost causing higher ranging error. Finally, it is interesting to note that the impact of system bandwidth has limitations in areas where heavier construction and obstacles separate sensor nodes. This can be seen by comparing the

impact of bandwidth on the localization performance in Schussler and Fuller.

5. CONCLUSION

In this paper, we provided an analysis of cooperative localization bounds for WSNs based on empirical models of UWB TOA-based OTI and ITI ranging in indoor multipath environments. We verified the need for cooperative localization in applications where indoor sensor nodes lack sufficient coverage to outdoor anchor nodes. We also verified that in addition to extending coverage, cooperative localization has potential for improving accuracy. In addition, we provided a comprehensive evaluation of the limitations imposed by the indoor multipath environment on cooperative localization performance in multihop WSNs.

Simulation results showed that increasing node density improves localization accuracy and can improve performance in indoor multipath channels. Increasing the number of anchors, however, has greater impact on harsh indoor en-vironments, such as office buildings, due to shorter ranging coverage, that is, less internode connectivity. For the ranging model parameters, localization is constrained by the ranging coverage, statistics of ranging error, probability of NLOS, probability of DP blockage, and bandwidth. In general, office building structures introduce higher probability of NLOS/DP blockage and shorter ranging coverage (higher DP penetration loss and pathloss exponent) which means higher localization error. Manufacturing floors and residential buildings, on the other hand, exhibit better performance due to "lighter" indoor channel conditions. Also, increasing the system bandwidth, although reduces ranging coverage, has the effect of improving accuracy. The localization performance in office buildings exhibited less sensitivity to changes in bandwidth because the range measurements faced harsher obstacles such as metallic doors, vending machines, and elevators.

As for the cooperative localization application for firefighter or military operations, it is clear that in order to improve accuracy, numerous nodes must be deployed in the indoor environment alongside those attached to the personnel. In addition to providing the necessary network density required for effective localization, these stationary nodes can constantly provide ranging/localization information which further improves performance in dense cluttered environments.

Future work in this area should aim to extend the analysis to 3 dimensions where RTI ranging can provide coverage extension to multifloor buildings. Further measurements and modeling are needed to analyze the ranging error beyond ranging coverage. Specifically, the behavior of the biases and measurement time variations with distance must be evaluated for different ranging scenarios and environments. Finally, research in localization algorithms for indoor-specific WSNs is needed to identify and mitigate NLOS biased range measurements in order to achieve acceptable localization performance.

REFERENCES

[1] I. F. Akyildiz, W. Su, Y. Sankarasubramaniam, and E. Cayirci, "A survey on sensor networks," *IEEE Communications Magazine*, vol. 40, no. 8, pp. 102–114, 2002.

[2] N. Patwari, J. N. Ash, S. Kyperountas, A. O. Hero III, R. L. Moses, and N. S. Correal, "Locating the nodes: cooperative localization in wireless sensor networks," *IEEE Signal Processing Magazine*, vol. 22, no. 4, pp. 54–69, 2005.

[3] K. Pahlavan, F. O. Akgül, M. Heidari, A. Hatami, J. M. Elwell, and R. D. Tingley, "Indoor geolocation in the absence of direct path," *IEEE Wireless Communications*, vol. 13, no. 6, pp. 50–58, 2006.

[4] K. Pahlavan, X. Li, and J.-P. Mäkelä, "Indoor geolocation science and technology," *IEEE Communications Magazine*, vol. 40, no. 2, pp. 112–118, 2002.

[5] S. Gezici, Z. Tian, G. B. Giannakis, et al., "Localization via ultra-wideband radios: a look at positioning aspects of future sensor networks," *IEEE Signal Processing Magazine*, vol. 22, no. 4, pp. 70–84, 2005.

[6] M. Ghavami, L. B. Michael, and R. Kohno, *Ultra-Wideband Signals and Systems in Communication Engineering*, John Wiley & Sons, Hoboken, NJ, USA, 2004.

[7] I. Oppermann, M. Hämäläinen, and J. Iinatti, Eds., *UWB Theory and Applications*, John Wiley & Sons, Hoboken, NJ, USA, 2004.

[8] D. Porcino and W. Hirt, "Ultra-wideband radio technology: potential and challenges ahead," *IEEE Communications Magazine*, vol. 41, no. 7, pp. 66–74, 2003.

[9] J.-Y. Lee and R. A. Scholtz, "Ranging in a dense multipath environment using an UWB radio link," *IEEE Journal on Selected Areas in Communications*, vol. 20, no. 9, pp. 1677–1683, 2002.

[10] K. Pahlavan, P. Krishnamurthy, and J. Beneat, "Wideband radio propagation modeling for indoor geolocation applications," *IEEE Communications Magazine*, vol. 36, no. 4, pp. 60–65, 1998.

[11] R. J. Fontana and S. J. Gunderson, "Ultra-wideband precision asset location system," in *Proceedings of IEEE Conference on Ultra-Wideband Systems and Technologies (UWBST '02)*, pp. 147–150, Baltimore, Md, USA, May 2002.

[12] W. C. Chung and D. Ha, "An accurate ultra-wideband ranging for precision asset location," in *Proceedings of IEEE Conference on Ultra-Wideband Systems and Technologies (UWBST '03)*, pp. 389–393, Reston, Va, USA, November 2003.

[13] B. Alavi and K. Pahlavan, "Modeling of the TOA-based distance measurement error using UWB indoor radio measurements," *IEEE Communications Letters*, vol. 10, no. 4, pp. 275–277, 2006.

[14] Z. Tarique, W. Q. Malik, and D. J. Edwards, "Bandwidth requirements for accurate detection of direct path in multipath environment," *Electronics Letters*, vol. 42, no. 2, pp. 100–102, 2006.

[15] E. G. Larsson, "Cramér-Rao bound analysis of distributed positioning in sensor networks," *IEEE Signal Processing Letters*, vol. 11, no. 3, pp. 334–337, 2004.

[16] A. Savvides, W. L. Garber, R. L. Moses, and M. B. Srivastava, "An analysis of error inducing parameters in multihop sensor node localization," *IEEE Transactions on Mobile Computing*, vol. 4, no. 6, pp. 567–577, 2005.

[17] C. Chang and A. Sahai, "Cramér-Rao-type bounds for localization," *EURASIP Journal on Applied Signal Processing*, vol. 2006, Article ID 94287, 13 pages, 2006.

[18] H. Koorapaty, H. Grubeck, and M. Cedervall, "Effect of biased measurement errors on accuracy of position location methods," in *Proceedings of IEEE Global Telecommunications Conference (GLOBECOM '98)*, vol. 3, pp. 1497–1502, Sydney, Australia, November 1998.

[19] C. Botteron, A. Host-Madsen, and M. Fattouche, "Effects of system and environment parameters on the performance of network-based mobile station position estimators," *IEEE Transactions on Vehicular Technology*, vol. 53, no. 1, pp. 163–180, 2004.

[20] Y. Qi, H. Kobayashi, and H. Suda, "Analysis of wireless geolocation in a non-line-of-sight environment," *IEEE Transactions on Wireless Communications*, vol. 5, no. 3, pp. 672–681, 2006.

[21] D. B. Jourdan, D. Dardari, and M. Z. Win, "Position error bound for UWB localization in dense cluttered environments," in *Proceedings of IEEE International Conference on Communications (ICC '06)*, vol. 8, pp. 3705–3710, Istanbul, Turkey, June 2006.

[22] D. B. Jourdan, D. Dardari, and M. Z. Win, "Position error bound and localization accuracy outage in dense cluttered environments," in *Proceedings of the IEEE International Conference on Ultra-Wideband*, pp. 519–524, Waltham, Mass, USA, September 2006.

[23] N. Alsindi, B. Alavi, and K. Pahlavan, "Empirical pathloss model for indoor geolocation using UWB measurements," *Electronics Letters*, vol. 43, no. 7, pp. 370–372, 2007.

[24] N. Alsindi, B. Alavi, and K. Pahlavan, "Spatial characteristics of UWB TOA-based ranging in indoor multipath environments," in *Proceedings of the IEEE International Symposium on Personal Indoor and Mobile Radio Communications (PIMRC '07)*, Athens, Greece, September 2007.

[25] N. Alsindi, B. Alavi, and K. Pahlavan, "Measurement and modeling of UWB TOA-based ranging in indoor multipath environments," to appear in *IEEE Transactions on Vehicular Technology*.

[26] K. Pahlavan and A. H. Levesque, *Wireless Information Networks*, John Wiley & Sons, New York, NY, USA, 2nd edition, 2005.

[27] P. Krishnamurthy and K. Pahlavan, "Analysis of the probability of detecting the DLOS path for geolocation applications in indoor areas," in *Proceedings of the 49th IEEE Vehicular Technology Conference (VTC '99)*, vol. 2, pp. 1161–1165, Houston, Tex, USA, May 1999.

[28] G. Durgin, T. S. Rappaport, and H. Xu, "Measurements and models for radio pathloss and penetration loss in and around homes and trees at 5.85 GHz," *IEEE Transactions on Communications*, vol. 46, no. 11, pp. 1484–1496, 1998.

[29] A. F. Molisch, "Ultra-wideband propagation channels-theory, measurement, and modeling," *IEEE Transactions on Vehicular Technology*, vol. 54, no. 5, pp. 1528–1545, 2005.

[30] S. S. Ghassemzadeh, R. Jana, C. W. Rice, W. Turin, and V. Tarokh, "Measurement and modeling of an ultra-wide bandwidth indoor channel," *IEEE Transactions on Communications*, vol. 52, no. 10, pp. 1786–1796, 2004.

[31] K. Siwiak, H. Bertoni, and S. M. Yano, "Relation between multipath and wave propagation attenuation," *Electronics Letters*, vol. 39, no. 1, pp. 142–143, 2003.

[32] M. Heidari, F. O. Akgül, and K. Pahlavan, "Identification of the absence of direct path in indoor localization systems," in *Proceedings of IEEE International Symposium on Personal Indoor and Mobile Radio Communications (PIMRC '07)*, Athens, Greece, September 2007.

[33] I. Guvenc, C.-C. Chong, and F. Watanabe, "NLOS identification and mitigation for UWB localization systems," in *Proceedings of the IEEE Wireless Communications and Networking Conference (WCNC '07)*, pp. 1571–1576, Kowloon, China, March 2007.

[34] H. L. Van Trees, *Detection, Estimation and Modulation Theory, Part I*, John Wiley & Sons, New York, NY, USA, 1968.

[35] S. Al-Jazzar, "Algorithms and parameter estimation for radiolocation in NLOS environments," Ph.D. dissertation, University of Cincinnati, Cincinnati, Ohio, USA, 2004.